Mechanical Degradation and Changes in Conformation of Hydrophobically Modified Starch

Lars Nilsson,*,† Mats Leeman,‡ Karl-Gustav Wahlund,‡ and Björn Bergenståhl†

Division of Food Technology and Division of Technical Analytical Chemistry, Centre for Chemistry and Chemical Engineering, Lund University, P.O. Box 124, S-221 00 Lund, Sweden

Received April 16, 2006; Revised Manuscript Received June 21, 2006

In this paper, we study the mechanical degradation and changes in conformation of a branched ultrahigh molar mass biomacromolecule, hydrophobically modified starch, as caused by high-pressure homogenization. The characterization was performed with asymmetrical flow field-flow fractionation (AsFlFFF) with multiangle light scattering (MALS) and refractive index detection. The starch which had been chemically modified with octenyl succinate anhydride (OSA) proved to be very large and polydisperse. Upon high-pressure homogenization, the molar mass and rms radius (r_{rms}) decreased, and the extent of these changes was related to the turbulent flow conditions during homogenization. The treatment also induced an increase and scaling with size in the apparent density of the macromolecules. To further study the changes in conformation, it was necessary to calculate the hydrodynamic radii (r_h). This can be determined numerically from the elution times in the analysis and the flow conditions in the AsFlFFF channel. The results showed that the treatment can cause a dramatic decrease in the quotient between r_{rms} and r_h, suggesting major conformational changes. These results together could be interpreted as degradation and “crumpling” of the macromolecule, which would give a decrease in r_{rms} and an increase in apparent density, together with a “fraying” of more outer parts of the macromolecule, which could give rise to the increase in r_h.

1. Introduction

In emulsions and other disperse systems, macromolecules are commonly used to provide colloidal stability. Macromolecules can act in favor of colloidal stability either by adsorbing to emulsion droplets to give steric and in some cases electrostatic stabilization or by increasing the viscosity of the continuous phase. For both steric and viscous stabilization, the molar mass distribution of the macromolecule is important, as it will affect the adsorption behavior and the ability to provide steric stabilization, as well as the ability to act as a thickener.

Hydrophobically modified starch, such as octenyl succinate anhydride (OSA) starch,[1] is an amphiphilic macromolecule, and it offers properties that have many applications within the formation and stabilization of dispersions. Through the chemical modification, the starch obtains substituents which contain both hydrophobic and anionic properties. The degree of substitution in food applications typically ranges downward from approximately 0.02.[2] Due to its high molar mass and branched polymer structure, hydrophobically modified starch that is adsorbed at the interface will give rise to steric stabilization, and it is possible to produce stable emulsions already at low OSA−starch concentrations.[3,4] The OSA−starch can also act as an associative thickener and thus can be used to change the rheological characteristics of a system.[5]

High-pressure homogenization is a commonly used device in many technical applications such as the formation of emulsions. In this process, as well as in many other processes used for emulsification, turbulent flow plays an important role for the disruption of the disperse phase.[6]

It is known that intense mechanical treatment, such as high-pressure homogenization, can influence the molar mass distribution and functionality of macromolecules. The degradation of polymers due to mechanical stress has been studied earlier by several authors.[7−11] Harrington and Zimm used viscometry to study the degradation of polystyrene during passage through a piston−cylinder apparatus and found that the critical stress for degradation of the polymer depended upon the solvent used, i.e., how stretched the polymer chain was.[7] Buchholz et al. investigated the possibility of narrowing the polydispersity of different high molar mass polymers by injecting the polymers in a capillary under high pressure.[8] The authors found a decrease in the polydispersity and the average molar mass, which were analyzed with size exclusion chromatography connected to multiangle light scattering detection (SEC-MALS). The phenomenon was interpreted to be of a physical nature and independent of the chemical nature of the polymers investigated. Furthermore, it was suggested that scission occurred when the polymers exceeded a flow-field-dependent critical chain length.

Studies dealing with the disruption of polysaccharides have also been carried out. Silvestri and Gabrielson studied the degradation of gum tragacanth during high-pressure homogenization using a microfluidizer device.[9] The authors found that the intrinsic viscosity of samples decreased as the number of passages or pressure increased. High-pressure homogenization using a microfluidization device was also used by Kasaai et al. to study fragmentation of chitosan.[10] The results of this study showed that the extent of degradation increased with the applied homogenization pressure, and they also showed that the larger polymers were preferentially degraded. Floury et al. studied degradation of methylcellulose during high-pressure homogenization with size exclusion chromatography connected to multiangle light scattering and refractive index detection (SEC-MALS-RI) and viscometry.[11] The authors observed weaker

* Corresponding author. lars.nilsson@food.lth.se. Tel: +46 462229670. Fax: +46 462224622.
† Division of Food Technology.
‡ Division of Technical Analytical Chemistry.

10.1021/bm060367h CCC: $33.50
Published on Web 08/12/2006

thickening characteristics of the methylcellulose after high-pressure homogenization, which was coupled to a decrease in molar mass.

Reports on the effect of homogenization on the molar mass distribution of starch derivatives are scarce despite their importance in many applications. The reason may be the difficulties in studying the molar mass distribution of starch derivatives by SEC due to their often ultrahigh molar mass. However, in the past decade, an alternative size separation technique, asymmetrical flow field-flow fractionation (AsFlFFF) with multiangle light scattering (MALS) detection has shown its applicability to the determination of the molar mass distribution of ultrahigh molar mass polymers.[12−15] Hence, the molar mass distribution of starch derivatives is now more easily investigated.

In this study, five different OSA starches from potato and barley origin were examined by asymmetrical flow FFF (AsFlFFF) combined with MALS and refractive index (RI) detection. The aim was to determine if high-pressure homogenization affects the molar mass distribution and conformation of OSA−starch. To do this, it was necessary to calculate the hydrodynamic radius (r_h) of the sample from the elution times obtained in the AsFlFFF analysis.

2. Experimental Section

2.1. Solutions of OSA−Starch. Five OSA−starch samples varying in molar mass, degree of substitution, and botanical origin were provided by Lyckeby Stärkelsen (Kristianstad, Sweden). The samples were from either native potato containing 80% amylopectin or high-amylopectin barley containing 93% amylopectin. The degree of substitution was determined with ^{1}H NMR.[4]

OSA−starch solutions of 1% (w/v) were prepared by dispersing 1.0 g of OSA−starch in a 10 mM phosphate buffer (pH 6.0) containing 20 ppm NaN_3, which was then diluted to 100 mL. The samples were then placed in a boiling water bath with stirring for 10 min after which they were left overnight at room temperature. The result was samples which ranged from a clear solution to a rather opaque "solution".

Half of each of the three sample solutions were then homogenized in a high-pressure lab-scale valve homogenizer at 15 MPa, while the other half of the solutions were kept nonhomogenized. The homogenizations were carried out at room temperature. The lab-scale homogenizer was equipped with a ball valve of stainless steel and has been described in detail elsewhere.[16] Solutions of homogenized and nonhomogenized samples were subsequently diluted to 0.025% (w/w) or 0.1% (w/w) in the carrier liquid prior to FFF analysis.

2.2. Analysis Equipment. The AsFlFFF instrument was an Eclipse F Separation System (Wyatt Technology, Santa Barbara, CA) which is an asymmetrical-flow FFF instrument. It was connected to a Dawn DSP Laser Photometer (Wyatt Technology), which is a multiangle light scattering (MALS) detector, and an Optilab DSP Interferometric Refractometer (Wyatt Technology), which is a refractive index (RI) detector. Both used a wavelength of 632.8 nm. An Agilent 1100 Series Isocratic Pump (Agilent Technologies, Waldbronn, Germany) with an in-line vacuum degasser and an Agilent 1100 Series Autosampler delivered the carrier flow and handled sample injection onto the AsFlFFF channel. Between the pump and the channel was placed a filter-holder in Teflon (made in-house) with a 20 nm pore-size aluminum oxide filter (Anodisc 25 cat. no. 6809-6002, Whatman International, Maidstone, U.K.) to ensure that particle free carrier entered the channel. Between the channel and the MALS detector was placed a PEEK precolumn filter with a 2 μm PEEK frit (cat. no. A·355 and A·700, Upchurch Scientific, Oak Harbor, WA) to remove large-sized impurities, which would otherwise disturb the MALS measurement and possibly clog the RI detector. The AsFlFFF channel had a nominal thickness of 250 μm, and the actual thickness was determined to be 193 μm by calibration against ferritin according to the procedure described in the literature.[17] The ultrafiltration membrane forming the accumulation wall was made of regenerated cellulose with a cutoff of 10 kDa (Nadir C010F, Microdyn-Nadir GmbH, Wiesbaden, Germany).

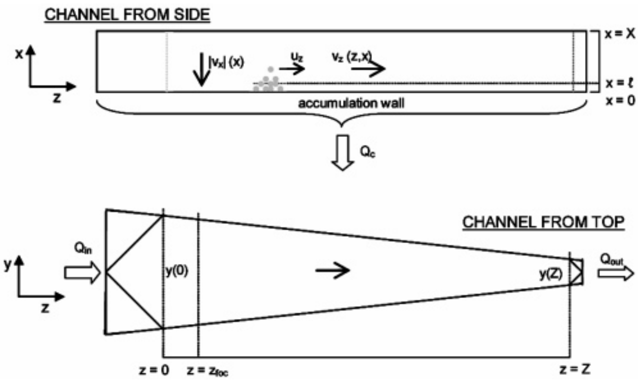

Figure 1. Side and top views of the FFF channel at a given time where v_x is the cross-flow velocity, $v_z(z, x)$ is the longitudinal flow velocity, x is the distance from the accumulation wall, Q_c is the volumetric cross-flow rate, Q_{in} is the inlet volumetric flow rate, Q_{out} outlet volumetric flow rate, z is the longitudinal position in the channel, and z_{foc} is the sample focusing point (in this case, 0.03 m).

2.3. Separation Parameters and Molar Mass Calculation Procedures. The sample injection onto the channel was commenced at a flow rate of 0.20 mL·min^{-1} during 1.0 min to rinse the sample loop. The OSA sample volume injected onto the channel was 10 μL for nonhomogenized OSA solutions and 40 μL homogenized OSA solutions for an injected mass of approximately 10 μg. A 3 min focusing/relaxation step was performed prior to elution with the focusing flow rate being identical to the initial cross-flow rate during elution, 1.0 mL·min^{-1}. To allow faster separation, a programmed cross-flow rate was used according to the function

$$Q_c(t) = Q_c(0) \cdot e^{-\frac{\ln 2}{t_{1/2}}t} \tag{1}$$

where $Q_c(t)$ is the cross-flow rate as a function of time t after the elution mode starts. The elution was started at an initial cross-flow rate $Q_c(0)$, of 1.0 mL·min^{-1}, and then decreased exponentially with a time constant, e.g., half-life, $t_{1/2}$, of 4 min. After 24 min of elution, the cross-flow was set to zero and the channel flushed without any cross-flow for 5 min before the next analysis. Detector flow rate was constant at 1.0 mL·min^{-1} throughout the separation. The carrier liquid for the separation was 10 mM $NaNO_3$ dissolved in water purified with a Milli-Q system (Millipore Corp., Bedford, MA) with 0.002% (w/v) NaN_3 added to prevent microorganisms from growing in the carrier. The carrier was filtered through a 0.2 μm pore-size regenerated cellulose filter (ord. no. 18407, Sartorious AG, Goettingen, Germany) prior to use.

Processing of light scattering data was made by the Astra software, version 4.73 (Wyatt Technology). The molar mass and the rms radius were obtained by Berry's method[18] fitting a straight line to the data obtained at 43−90° scattering angle. The lowest scattering angles, 14−35°, were not included, as these data were too imprecise. A dn/dc value of 0.146 mL·g^{-1} was used,[19] and the second virial coefficient was assumed to be negligible. The dn/dc for the OSA−starch samples was not determined, but as the substances consists of >97% starch, any difference in dn/dc value compared to other starches is small.

3. Theory

3.1. Calculation of the Hydrodynamic Radius. In field-flow fractionation with a constant cross-flow, the diffusion coefficient of an eluted component can be calculated if the cross-

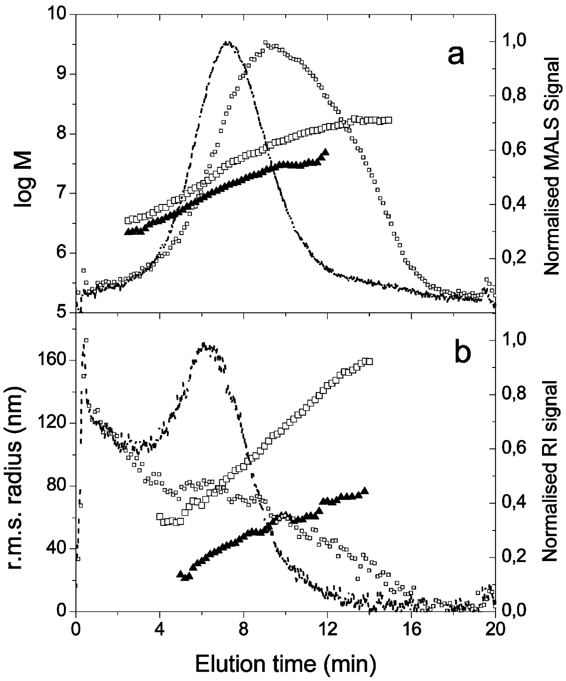

Figure 2. The logarithm of the molar mass (g/mol) vs elution time (a) and rms radius vs elution time (b) for homogenized and nonhomogenized OSA−starch B39-22. The symbols denote as follows: □, nonhomogenized sample; ▲ homogenized sample; small box, detector signals for the nonhomogenized sample; and the dashed line denotes the detector signals for the homogenized sample. The detector signals are the fractograms obtained from the MALS photometer at 90° angle (a) and the RI detector (b).

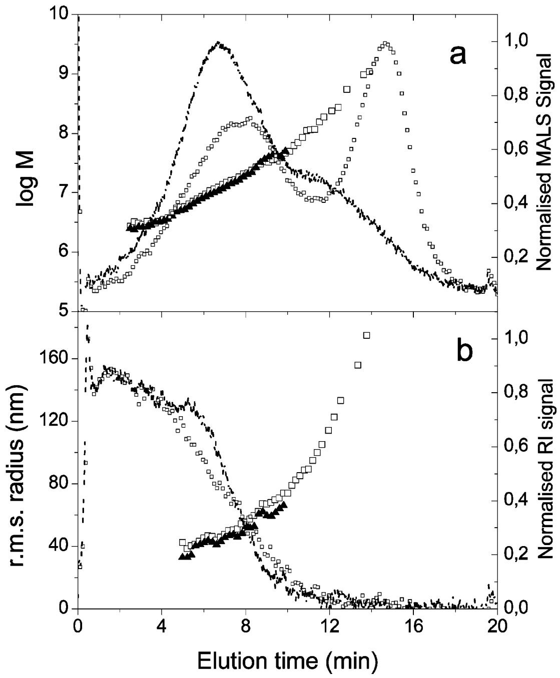

Figure 3. The logarithm of the molar mass (g/mol) vs elution time (a) and rms radius vs elution time (b) for homogenized and nonhomogenized OSA−starch B27-21. The symbols denote as follows: □, nonhomogenized sample; ▲, homogenized sample; small box, detector signals for the nonhomogenized sample; and the dashed line denotes the detector signals for the homogenized sample. The detector signals are the fractograms obtained from the MALS photometer at 90° angle (a) and the RI detector (b).

flow rate and channel dimensions are known.[13] The diffusion coefficient is in this case proportional to the inverse of the retention time. The r_h can then be obtained from the Stokes−Einstein equation[20]

$$r_h = \frac{kT}{12\pi\eta D} \tag{2}$$

where k is Boltzmann's constant, T is the temperature, η is the viscosity of the solvent, and D is the diffusion coefficient. However, when using an exponentially decaying cross-flow, the determination of r_h becomes more difficult as the flow-field decreases with time. Another phenomenon that further complicates the determination of r_h under this condition is the so-called secondary relaxation effect,[21] which is attributed to the finite time it takes for components to relax by diffusion away from the accumulation wall when the cross-flow is decreased. Figure 1 shows a schematic of the channel used in the experiments from top and side views, respectively.

From the dimensions of the channel and the flow conditions, it is possible to derive an expression for the elution time of a component and thus its diffusion coefficient. This has been done previously for a rectangular channel by Kirkland et. al.[22] In our case, the expression becomes more complicated due to the trapezoidal geometry of the channel. The distance traveled along the channel, dz, by a component during the time dt is equal to the velocity u_z of the component as

$$\mathrm{d}z = u_z(z, x, t)\cdot \mathrm{d}t \tag{3}$$

The longitudinal velocity of the carrier liquid is dependent on the distance, x, from the wall and the cross-average longitudinal flow velocity, $\overline{v_z}(z, t)$. By assuming a laminar flow with a parabolic velocity profile, u_z can be described by

$$u_z(z, x, t) = 6\cdot\overline{v_z}(z, t)\cdot\left[\frac{x}{X} - \frac{x^2}{X^2}\right] \tag{4}$$

where X refers to the thickness of the channel which is assumed to be constant.

The average distance of a component from the channel accumulation wall, l, is related to the diffusion coefficient, D, of the component and the transversal (cross) flow velocity, v_x, at the accumulation wall. When $x \ll X$, this can approximated as

$$l = \frac{D}{|v_x(t)|} \tag{5}$$

As long as the pressure drop along the channel remains much less than the pressure drop across the accumulation wall, v_x will be independent of z, and we obtain

$$v_x(z, t) = v_x(t) \tag{6}$$

and the total volumetric flow can be expressed as

$$Q_c(t) = v_x(t)\cdot A \tag{7}$$

where $Q_c(t)$ is the volumetric flow rate and A is the total area of the accumulation wall.

By combining eqs 3−7, we obtain

$$u_z(z, t) = 6\cdot\overline{v_z}(z,t)\cdot\left[\frac{DA}{Q_c(t)\cdot X} - \frac{D^2A^2}{Q_c^{\,2}(t)\cdot X^2}\right] \tag{8}$$

CDV

The cross-average longitudinal velocity depends on the position along the channel, as part of the carrier liquid is continuously exiting through the accumulation wall. The cross-flow that has already left the channel before point z, $Q_c(z)$, is given by

$$Q_c(z, t) = |v_x(t)|\cdot A(z) \tag{9}$$

where $A(z)$ is the area of the accumulation wall up to z, and by using eq 7, we obtain

$$Q_c(z, t) = Q_c(t)\,\frac{A(z)}{A} \tag{10}$$

The volumetric longitudinal flow at point z, Q_z, then becomes the inlet flow, Q_{in}, minus the volumetric cross-flow that has left up to z, $Q_c(z, t)$, and as $Q_{in} = Q_{out} + Q_c(t)$, this can be written as

$$Q_z(z, t) = Q_{out} + Q_c(t)\left(1 - \frac{A(z)}{A}\right) \tag{11}$$

The cross-average velocity in the longitudinal velocity at point z in the channel can then be obtained by dividing the volumetric flow rate by the cross-sectional area

$$\overline{v_z}(z, t) = \frac{Q_{out} + Q_c(t)\left(1 - \dfrac{A(z)}{A}\right)}{X\cdot y(z)} \tag{12}$$

where X is the channel thickness and $y(z)$ is the channel breadth at point z. For a trapezoidal channel as depicted above, the breadth at position z between the tapered inlet and outlet can be described by the following:

$$y(z) = y(0) - [y(0) - y(Z)]\cdot\frac{z}{Z} \tag{13}$$

By combining eqs 8 and 12, the following differential equation is obtained

$$u_z(z, t) = \frac{dz}{dt} = 6\cdot\frac{Q_{out} + Q_c(t) - Q_c(t)\cdot\dfrac{A(z)}{A}}{X\cdot y(z)}\cdot\left[\frac{DA}{Q_c(t)\cdot X} - \frac{D^2A^2}{Q_c^{\,2}(t)\cdot X^2}\right] \tag{14}$$

which describes the velocity of a sample component in direction z over time.

The area of the accumulation wall up to a point z, $A(z)$, can be expressed by

$$A(z) = A_{inlet} + z\left[\frac{y(0) + y(Z)}{2}\right] = A_{inlet} + z\left[\frac{y(0) + [y(0) - y(Z)]\cdot z/Z}{2}\right] \tag{15}$$

where A_{inlet} is the area of the accumulation wall before its widest point $y(0)$. In our case, the cross-flow rate is exponentially decaying with time according to eq 1.

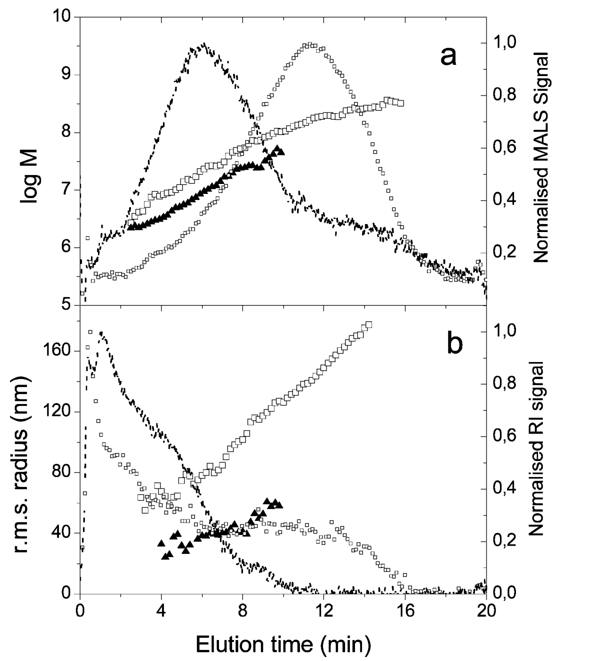

Figure 4. The logarithm of the molar mass (g/mol) vs elution time (a) and rms radius vs elution time (b) for homogenized and nonhomogenized OSA−starch B86-10. The symbols denote as follows: □, nonhomogenized sample; ▲, homogenized sample; small box, detector signals for the nonhomogenized sample; and the dashed line denotes the detector signals for the homogenized sample. The detector signals are the fractograms obtained from the MALS photometer at 90° angle (a) and the RI detector (b).

By inserting eqs 1, 13, and 15 into eq 14, we obtain the final expression

$$\frac{dz}{dt} = 6\cdot\frac{\dfrac{DA}{X\cdot Q_c(0)\cdot e^{-\frac{\ln 2}{t_{1/2}}t}} - \left(\dfrac{DA}{X\cdot Q_c(0)\cdot e^{-\frac{\ln 2}{t_{1/2}}t}}\right)^2}{X\cdot\left[(y(0) - [y(0) - y(Z)])\cdot\dfrac{z}{Z}\right]}\cdot\left[Q_{out} + Q_c(0)\cdot e^{-\frac{\ln 2}{t_{1/2}}t} - Q_c(0)\cdot e^{-\frac{\ln 2}{t_{1/2}}t}\cdot\left(\frac{A_{inlet}}{A} + \frac{z}{2A}\left[y(0) + (y(0) - [y(0) - y(Z)])\cdot\frac{z}{Z}\right]\right)\right] \tag{16}$$

The elution time of a component is when it has traveled from the focusing point $z = z_{foc}$, from where its migration toward the channel outlet starts, to the end of the channel $z = Z$.

Equation 16 is a differential equation of the form

$$\frac{dz}{dt} = \left[\frac{f(t) - g(t)\,h(z)}{i(z)}\right]k(t) \tag{17}$$

which can be solved numerically for every D in order to obtain t when z equals Z and thus the hydrodynamic radius through the Stokes−Einstein equation (eq 2). The solution is discussed in the Discussion section of this paper. Kirkland et al. arrived at a less complex differential equation, for a rectangular channel, which could be solved analytically.[22]

4. Results

The effect of high-pressure homogenization was evaluated for five OSA-modified starches of potato and barley. The molar mass and rms radius were determined with AsFlFFF-MALS-RI. Through this method, we were able to obtain the distributions

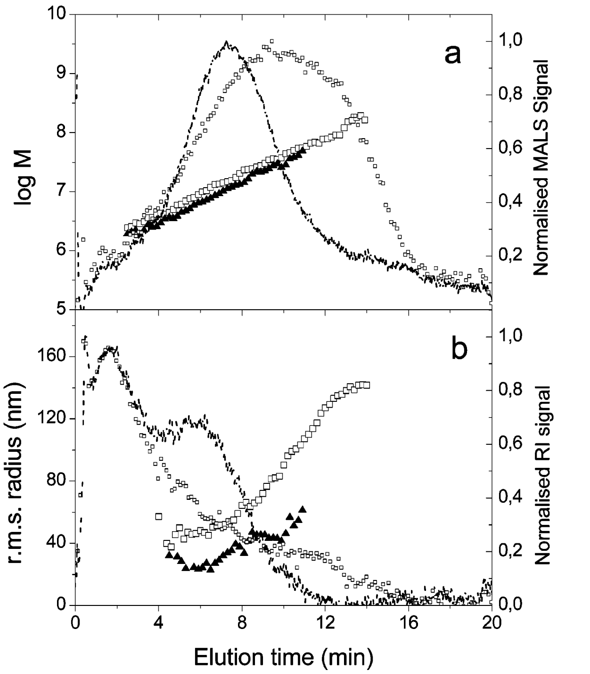

Figure 5. The logarithm of the molar mass (g/mol) vs elution time (a) and rms radius vs elution time (b) for homogenized and nonhomogenized OSA−starch P23-14. The symbols denote as follows: □, nonhomogenized sample; ▲, homogenized sample; small box, detector signals for the nonhomogenized sample; and the dashed line denotes the detector signals for the homogenized sample. The detector signals are the fractograms obtained from the MALS photometer at 90° angle (a) and the RI detector (b).

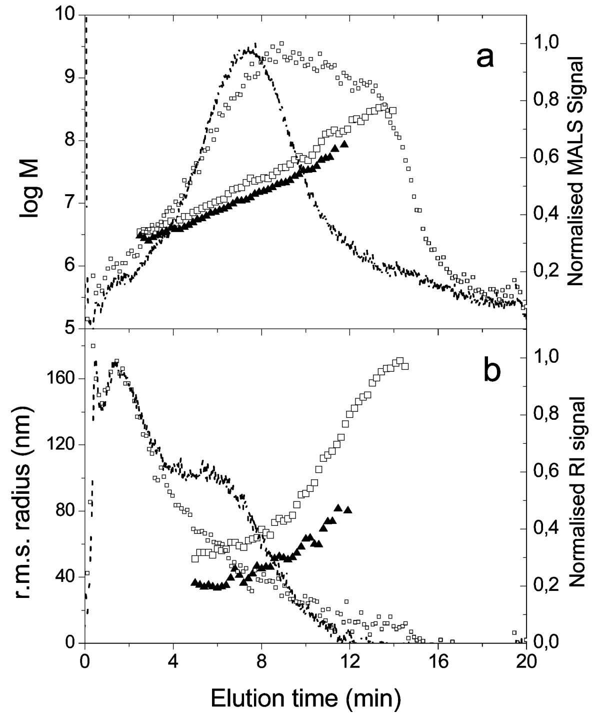

Figure 6. The logarithm of the molar mass (g/mol) vs elution time (a) and rms radius vs elution time (b) for homogenized and nonhomogenized OSA−starch P34-076. The symbols denote as follows: □, nonhomogenized sample; ▲, homogenized sample; small box, detector signals for the nonhomogenized sample; and the dashed line denotes the detector signals for the homogenized sample. The detector signals are the fractograms obtained from the MALS photometer at 90° angle (a) and the RI detector (b).

of molar mass and rms radius for the various samples before and after homogenization. Figures 2−6 show plots of the results for the homogenized and nonhomogenized OSA−starch samples. The graphs show that starch that had been chemically modified with OSA was a polydisperse polymer containing ultrahigh molar mass components reaching molar masses of 300 million g/mol. Furthermore, the plots show a shift in elution times depending on sample homogenization, that is, the homogenized samples are eluted earlier. The later eluted, larger, components present in the nonhomogenized samples were not detected or are less abundant after homogenization, which implies that the OSA−starch is affected by the high-pressure homogenization.

An overview of the results for the various samples is shown in Table 1. The molar mass and the rms radius results in Table 1 also summarize what is shown by the shift in AsFlFFF elution time, i.e., how the size of the OSA−starch is influenced by high-pressure homogenization. Both the average molar mass and the average r_{rms} decrease as a result of the treatment. The width of the molar mass distribution, given as the relative standard deviation SD_{rel}, has also decreased after homogenization, except for sample B86-10, where it is unaffected at a rather low value. The average r_{rms} values after homogenization have been reduced to a level that is similar between samples and independent of the size of the original sample.

AsFlFFF separates macromolecules according to differences in diffusion coefficient, i.e., hydrodynamic radius (r_h). Hence, two polymer fractions being eluted at identical times from the AsFlFFF channel (assuming the same separation conditions) thereby have the same diffusion coefficient. If the rms radius (determined by the MALS alone) and the molar mass (determined by the MALS-RI combination) for the fractions are the

Table 1. Overview of OSA−Starch Samples and the Averages Obtained from the FFF Analysis[a]

sample	DS	DB	Mw_i Mw range (10^6g/mol)	Mw_i SD_{rel}	Mw_f Mw range (10^6 g/mol)	Mw_f SD_{rel}	initial r_{rms} (nm)	final r_{rms} (nm)
B39−22	0.022	0.055	39	1.0	12	0.82	87	38
			3.3−140		2.3−48			
B27−21	0.021	0.050	27	3.6	8.6	0.99	52	44
			2.8−690		2.2−66			
B86−10	0.010	0.053	86	1.0	6.7	1.0	104	41
			2.8−320		1.6−34			
P23−14	0.014	0.035	23	1.5	8.8	0.86	69	32
			2.2−130		1.8−34			
P34−076	0.0076	0.035	34	2.0	11	0.95	75	42
			3.2−310		3.5−53			

[a] DS is the degree of substitution and DB is the degree of branching. The subscripts i and f denote initial and final average molar mass and refer to nonhomogenized and homogenized samples, respectively. Mw range is the molar mass range upon which Mw is based, and SD_{rel} is the relative standard deviation giving a measure of the polydispersity of the sample. r_{rms} is the root-mean-square radius before and after homogenization.

same, it indicates that the structures of the two polymers are similar. In Figures 2, 4, 5, and 6, a difference can be seen in the molar mass and r_{rms} at a given elution time of homogenized and nonhomogenized samples. The molar mass and r_{rms} appear smaller at the same elution time (hydrodynamic radius). This is true for samples B39-22, B86-10, and to a lesser extent for samples P23-14 and P34-076. As the flow conditions are identical, this suggests that the homogenization has caused a change in the conformational properties as well as in the actual molecular size of the sample. If one compares r_{rms} at a given elution time, it also differs for B39-22 and B86-10, and the difference is more pronounced for samples P23-14 and P34-076 compared to the relationship between elution time and molar mass.

5. Discussion

The results show that high-pressure homogenization affects the OSA−starch in several ways. The molar mass and root-mean-square radius decrease and the magnitude of the molar mass change caused by homogenization seems to depend on the initial molar mass. The higher the initial molar mass, the greater the change will be, and it is also clear that the difference in molar mass between the different samples is reduced after homogenization. Two possible explanations exist for the change in molar mass. It could be due to the breakage of covalent bonds, i.e., intramolecular, or it could be due to the disruption of aggregates, i.e., the breakage of intermolecular bonds. From the results within the current study, it is impossible to rule out any of these explanations, and it is therefore reasonable to assume that both the suggested mechanisms can occur. Due to the processing that the OSA−starch has undergone (i.e., chemical modification and high-pressure homogenization), it can be considered to contain not only the native starch components (amylose and amylopectin) but also degradation products. These degradation products can contain both linear and branched structures, and it is not possible to determine whether the early eluting components are amylose[23] or amylopectin fragments. The likeliest case is that it is both of the above.

The difference in r_{rms} is also reduced after the homogenization, and the averages of the samples are quite similar. It has been described by other authors that there seems to be a limiting size for polymers which depend on the processing conditions.[8,10,24,25]

High-pressure homogenization is usually an energy-intense process, and an essential processing parameter is the energy dissipation rate ϵ (W/kg). The energy dissipation rate depends mainly on the homogenization pressure and the volume in which the energy is dissipated. A typical value of ϵ for high-pressure homogenizers[6] is 10^9 W/kg. In the volume where the main homogenization occurs, the flow conditions are turbulent, and the flow can be assumed to be locally isotropic. This simplifies the description of the flow and the size range of the turbulent eddies, the Kolmogorov scale, can be estimated with the theories of Kolmogorov,[26] Levich,[27] and others

$$\lambda = \left(\frac{\nu^3}{\epsilon}\right)^{1/4} \tag{18}$$

where λ is the length scale of the smallest turbulent eddies, ν is the kinematic viscosity (m^2/s), and ϵ is the energy dissipation rate per unit mass (W/kg). As λ is obtained from scaling laws, it is important to remember that it only provides an estimate of the length scale of the turbulent eddies. On the basis of the approach above, the disruption of a macromolecule like OSA−starch would depend to a great extent on the turbulent eddies. To cause disruption of a macromolecule, the length scale of the turbulent eddies should be smaller than the length scale of the macromolecule, as the eddies then would generate a shear field over the macromolecule. This shear field could then ultimately lead to rupture of the macromolecule itself or of macromolecular aggregates. If, on the other hand, the length scale of the eddies is larger than the macromolecule, they would not cause any disruption. In our case, if we assume $\nu = 10^{-6}$ m^2/s and use $\epsilon = 10^9$ W/kg, then $\lambda \approx 180$ nm, which is on the same order of magnitude as the root-mean-square diameter of the homogenized samples. The estimation provides a possible explanation for the similarity in r_{rms} values between the various OSA−starch samples after homogenization.

One interesting observation from the result is the change in hydrodynamic radius in relation to the molar mass before and after homogenization. This is likely to be due to some change in the conformation of the OSA−starch. A physical characteristic that could be interesting to compare between samples before and after homogenization is the apparent density of the OSA−starch. This density can be obtained from the molar mass and rms radii distributions, assuming homogeneous distribution of mass and a spherical shape. As the rms radius gives only an approximate description of the volume of possible shapes, the density obtained should be considered an apparent property. The apparent density for component i of the sample ρ_i is given in eq 3

$$\rho_i = \frac{M_i}{V(r_{rms})_i} \cdot q \tag{19}$$

where M is the molar mass, V is the volume, and q is given by eq 4 where r is the radius of a sphere.

$$q = \frac{V_{sphere}(r_{rms})}{V_{sphere}(r)} = \frac{r_{rms}^3}{r^3} = \frac{(\sqrt{3/5} \cdot r)^3}{r^3} = \left(\frac{3}{5}\right)^{3/2} \tag{20}$$

The plots in Figure 7 show that the apparent density for the nonhomogenized samples is low (around 10 kg/m^3) and that it remains rather constant throughout the distribution.

The low magnitude suggests an aggregate structure with about 1−2% (v/v) segment density. The constant density as a function of size suggests a three-dimensional regularity (fractal dimensionality of 3) and a nonfractal structure. This result contradicts a random coil conformation as it would scale with size. We imagine this feature to be caused by a regular packing of three-dimensional units building up the molecule. However, after homogenization, the apparent density has increased for most samples, although the results show some variation. This increase in apparent density suggests that the molecules have become more compact after homogenization. Typical results correspond to a segment density of about 5% (v/v). A second feature is that the apparent density can be strongly dependent on the size of the molecule. Smaller molecules appear more compact and larger structures less compact, which is what would be expected for a random coil with fractal scaling.

The difference in elution behavior mentioned above cannot be explained by this result, as one would expect that an increase in the apparent density of an OSA−starch fraction should cause the elution time to become shorter for the specific fraction after homogenization. In our case, the opposite occurs, i.e., the elution time for a fraction of a specific molar mass either becomes longer or is unaffected by homogenization. To further investigate this phenomenon, one may study the hydrodynamic radius of

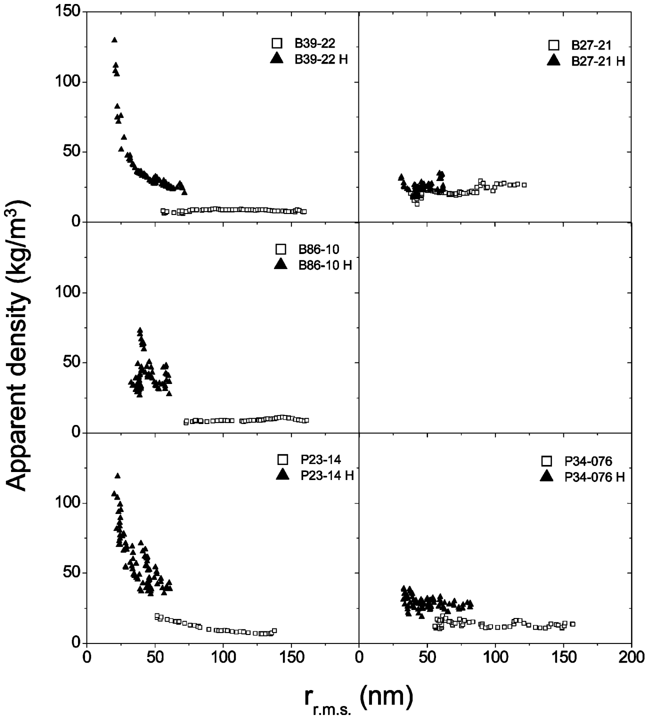

Figure 7. The apparent density of the various OSA−starch samples before and after homogenization (denoted with an H following the sample ID) vs the rms radius.

Table 2. Average Hydrodynamic Radius before (initial) and after (final) Homogenization for the Six OSA−Starch Samples

sample	initial r_h (nm)	final r_h (nm)
B39−22	40	37
B27−21	34	27
B86−10	53	22
P23−14	38	31
P34−076	35	34

Table 3. Calculated Values for the Quotient r_{rms}/r_h for Different Objects and Experimental Results from Literature

object	r_{rms}/r_h
hard (homogeneous) sphere	0.775
rod	
axial ratio = 20	1.729[30]
axial ratio = 100	2.659[30]
flexible polymer	
θ-solvent	1.506[30]
good solvent	1.862[30]
exptl results	
xanthan gum	2.17−2.95[31]
κ-carrageenan (coil)	1.96,[30] 1.44,[32] 1.65[33]
nonionic modified celluloses	1.71−2.64[34]
amylose	1.63−2.07[35]
amylopectin	1.02−1.29[36]

the samples and a useful qualitative measure in judging which conformational architectures that are present in a polymer solution is the quotient r_{rms}/r_h.[28] Values for some generalized conformations are given in Table 3.

The numerical solution of eq 19 was obtained using a Fehlberg fourth-fifth-order Runge−Kutta method[29] for diffusion coefficients between 10^{-10} and 10^{-12}. To compensate for the position in the channel where the elution of the sample starts, an initial condition was set to $t(0.03) = 0$. The results are plotted

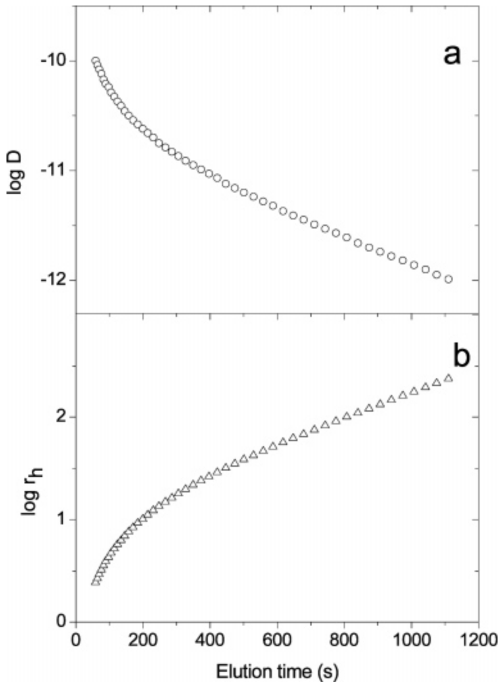

Figure 8. Plots of the numerical solution of eq 16 which shows the logarithm of the diffusion coefficient (D) vs elution time (a) and the logarithm of the hydrodynamic radius (r_h) vs elution time (b). The hydrodynamic radius was obtained from the Stokes−Einstein equation (eq 2). The intersection of the tangential function corresponds to the void time which is approximately 58 s.

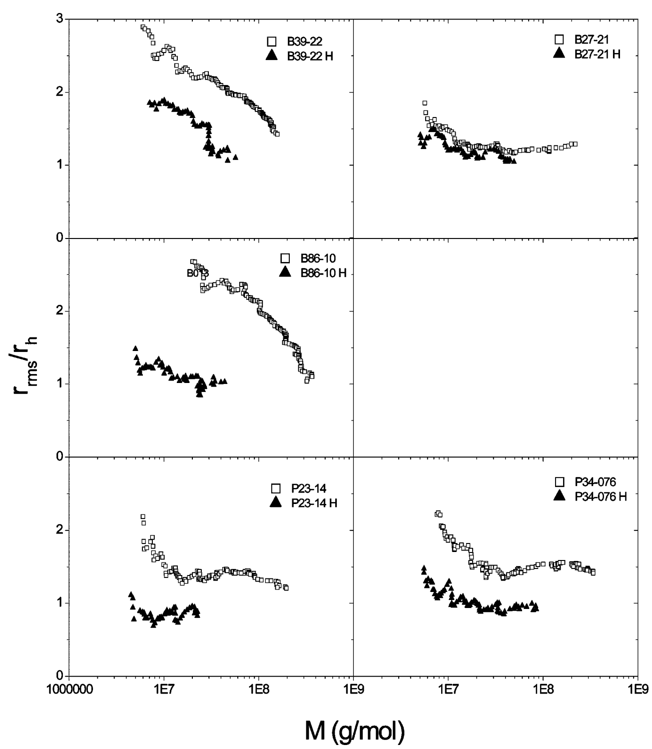

Figure 9. Plots of the quotient r_{rms}/r_h vs the logarithm of the molar mass of the various OSA−starch samples before and after high-pressure homogenization (denoted by H following the sample ID).

in Figure 8. To calculate the hydrodynamic radius for each time value obtained in the analysis, a polynomial fit was carried out on the function in Figure 8b. Table 2 gives the average r_h before and after homogenization.

Figure 9 shows r_{rms}/r_h vs log M for the various OSA−starch samples before and after homogenization. The plots show a

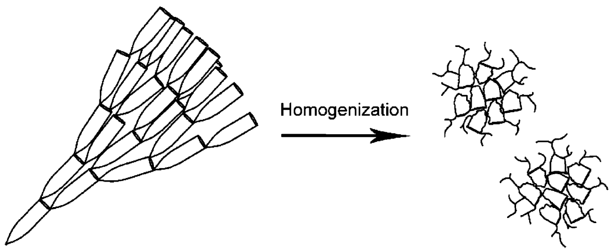

Figure 10. Schematic of hypothetical structures to illustrate changes caused by homogenization.

decrease in r_{rms}/r_h after homogenization in all cases except for the B27-21 sample. This indicates a major change in the conformational structure of the OSA–starch after homogenization. A lower r_{rms}/r_h ratio generally indicates a more compact structure (see Table 3), and the r_{rms}/r_h data thus support the density calculations suggesting that the homogenized OSA starch is denser than the initial. Furthermore, it can be observed that r_{rms}/r_h seems to depend on the molar mass of the OSA–starch.

In Table 3, some theoretical and experimental values of r_{rms}/r_h found in the literature are given as a comparison for the ones obtained for the various OSA–starch samples. The experimental values in Table 3 have been obtained through various light scattering techniques, and it can be said that there is fair amount of variation between results for similar macromolecules. As r_{rms}/r_h for the OSA–starch depends on the molar mass, this could indicate that several conformational structures are present within the same sample, and it is not straightforward to make a comparison with the values found in the literature. However, it is possible to conclude that the results obtained for OSA–starch fall within the same range as the results found for other polysaccharides. In some cases, like B39-22, the nonhomogenized samples display very high values for r_{rms}/r_h at low molar mass. This can be interpreted as a shape anisotropy toward elongated cylinders. A possible error that could cause these high values is the underestimation of r_h in the calculations above, which in turn might be due to orientation of the macromolecule in the FFF channel. Another possible error which might contribute is the secondary relaxation effect mentioned above.

6. Conclusion

Starch which has been hydrophobically modified with OSA is a polydisperse amphiphilic macromolecule which contains ultrahigh molar mass components. Upon high-pressure homogenization, the size and conformational characteristics of the macromolecules can change as the average molar mass and rms radius decrease. The polydispersity of the samples also decreases or remains at a low level as a result of homogenization. The extent of these changes seems to depend on the turbulent flow conditions during homogenization and thus on the energy dissipation rate in the homogenizer. Furthermore, the apparent density of the macromolecule can increase substantially after homogenization for molecules of a similar molar mass. This suggests that the molecules can become more compact as a result of high-pressure homogenization. The hydrodynamic properties of the OSA–starch can also change upon homogenization, and although the OSA–starch can become smaller and more compact as a result of homogenization, the change in elution behavior suggests a larger hydrodynamic size after homogenization for components of similar molar mass. This implies a change in conformation of the macromolecules, which can be qualitatively described as the quotient between r_{rms} and r_h of the macromolecule. The quotient r_{rms}/r_h can indeed become lower after homogenization, which shows that the relationship between hydrodynamic radius and rms radius has changed and thus the conformation of the macromolecule. These results together could be interpreted as degradation and "crumpling" of the macromolecule, which would give a decrease in r_{rms} and an increase in apparent density, together with a "fraying" of more outer parts of the molecule, which could give rise to the increase in r_h. These hypothetical structures are illustrated schematically in Figure 10. The degradation and changes in structural conformation are likely to influence the physical–chemical properties of the OSA–starch. The changes could for instance influence the surface activity and the adsorption behavior and thus the employment of the OSA–starch in different applications such as colloidal systems. However, this question remains to be answered and awaits further research.

Acknowledgment. Financial support from the Center for Amphiphilic Polymers from renewable resources, Lund, Sweden and the Swedish Research Council is gratefully acknowledged.

References and Notes

(1) Caldwell, C. G.; Wurzburg, O. B. U. S. Patent 2,661,349, 1953.
(2) Shogren, R. L.; Viswanathan, A.; Felker, F.; Gross, R. A. *Starch/Stärke* **2000**, *52*, 196–204.
(3) Tesch, S.; Gerhards, C.; Schubert, H. *J. Food Eng.* **2002**, *54*, 167–174.
(4) Nilsson, L.; Bergenståhl, B. Submitted for publication, 2006.
(5) Ortega-Ojeda, F. E.; Larsson, H.; Eliasson, A.-C. *Carbohydr. Polym.* **2005**, *59*, 313–327.
(6) Walstra, P. In *Encyclopedia of emulsion technology volume I: Basic Theory*; Becher, P., Ed.; Marcel Dekker Inc.: New York, 1983; pp 57–127.
(7) Harrington, R. E.; Zimm, B. H. *J. Phys. Chem.* **1965**, *69*, 161–175.
(8) Buchholz, B. A.; Zahn, J. A.; Kenward, M.; Slater, G. W.; Barron, A. E. *Polymer* **2004**, *45*, 1223–1234.
(9) Silvestri, S.; Gabrielson, G. *Int. J. Pharm.* **1991**, *73*, 163–169.
(10) Kasaai, M. R.; Charlet, G.; Paquin, P.; Arul, J. *Innovative Food Sci. Emerging Technol.* **2003**, *4*, 403–413.
(11) Floury, J.; Desrumaux, A.; Axelos, M. A. V.; Legrand, J. *Food Hydrocolloids* **2002**, *16*, 47–53.
(12) Wittgren, B.; Wahlund, K.-G. *J. Chromatogr., A* **1997**, *760*, 205–218.
(13) Andersson, M.; Wittgren, B.; Wahlund, K.-G. *Anal. Chem.* **2001**, *73*, 4852–4861.
(14) Roger, P.; Baud, B.; Colonna, P. *J. Chromatogr., A* **2001**, *917*, 179–185.
(15) Lee, S.; Nilsson, P.-O.; Nilsson, G. S.; Wahlund, K.-G. *J. Chromatogr., A* **2003**, *1011*, 111–123.
(16) Tornberg, E.; Lundh, G. *J. Food Sci.* **1978**, *43*, 1553–1558.
(17) Wahlund, K. G. In *Field-flow fractionation handbook*; Schimpf, M. E., Caldwell, K., Giddings, J. C., Eds.; John Wiley & Sons, Inc.: New York, 2000.
(18) Berry, G. C. *J. Chem. Phys.* **1966**, *44*, 4450–4564.
(19) Brandrup, J., Immergut, E. H., Grulke, E. A., Eds. *Polymer Handbook*, 4th ed.; John Wiley & Sons: New York, 1999.
(20) Einstein, A. *Ann. Phys.* **1905**, *17*, 549–560.
(21) Williams, P. S. In *Field-Flow Fractionation Handbook*; Schimpf, M. E., Caldwell, K., Giddings, J. C., Eds.; John Wiley & Sons, Inc.: New York, 2000.
(22) Kirkland, J. J.; Dilks, C. H., Jr.; Rementer, S. W.; Yau, W. W. *J. Chromatogr.* **1992,** *593*, 339–355.
(23) Leeman, M.; Wahlund, K. G. Unpublished results.
(24) Striegel, A. M. *J. Biochem. Biophys. Methods* **2003**, *56*, 117–139.
(25) Modig, G.; Nilsson, L.; Bergenståhl, B.; Wahlund, K. G. *Food Hydrocolloids* **2006**, *20*, 1087–1095.
(26) Kolmogorov, A. N. *Dokl. Akad. Nauk SSSR* **1949**, *66*, 825–828.
(27) Levich, V. G. *Physicochemical hydrodynamics*; Prentice Hall: Englewood Cliffs, NJ, 1962.
(28) Burchard, W. *Adv. Polym. Sci.* **1999**, *143*, 113–194.
(29) Forsythe, G. E.; Malcolm, M. A.; Moler, C. B. *Computer methods for mathematical computations*; Prentice Hall: Englewood Cliffs, NJ, 1977.

CDV

(30) Wittgren, B.; Borgström, J.; Piculell, L.; Wahlund, K. G. *Biopolymers* **1998**, *45*, 85−96.
(31) Coviello, T.; Kajiwara, K.; Burchard, W.; Dentini, M.; Crescenzi, V. *Macromolecules* **1986**, *19*, 2826−2831.
(32) Drifford, M.; Tivant, P.; Bencheikh-Larbi, F.; Tabti, K.; Rochas, C.; Rinaudo, M. *J. Phys. Chem.* **1984**, *88*, 1414−1420.
(33) Viebke, C.; Williams, P. A. *Food Hydrocolloids* **2000**, *14*, 265−270.
(34) Nilsson, S.; Sundelöf, L.-O.; Porsch, B. *Carbohydr. Polym.* **1995**, *28*, 265−275.
(35) Roger, P.; Colonna, P. *Carbohydr. Res.* **1992**, *227*, 73−83.
(36) Roger, P.; Bello-Perez, L. A.; Colonna, P. *Polymer* **1999**, *40*, 6897−6909.

BM060367H